JOURNAL OF AIRCRAFT
Vol. 45, No. 2, March–April 2008

Buckling Behavior of Composite Laminated Stiffened Panels Under Combined Shear–Axial Compression

H. Abramovich* and T. Weller†
Technion—Israel Institute of Technology, 32000 Haifa, Israel
and
C. Bisagni‡
Politecnico di Milano, 20156 Milano, Italy

DOI: 10.2514/1.27635

Experimental results are reported on the behavior of four torsion boxes, each comprising two stringer-stiffened cylindrical graphite-epoxy composite panels that were subjected to torsion, axial loading, and their combinations. The buckling and postbuckling behavior of these torsion boxes demonstrated consistent results. Before performing the buckling tests, the initial geometric imperfections of the panels forming the boxes were scanned and recorded. The tests were complemented by finite element calculations that were performed for each box. These detailed calculations also assisted in identifying critical regions of the boxes, and the boxes were reinforced accordingly, to avoid their premature failure. The tests indicated that the torsion-carrying capacity was dependent on stringer geometry and layup; axial compression results were in very good agreement with previous tests carried out with single identical panels; and the boxes have a very high postbuckling-carrying capacity. Comparisons of the experimentally experienced first (skin) buckling loads and collapse torques with finite element analyses predictions were found to be in good agreement for torsion and for axial compression. The experimental results under combined loading were consistently lower than with the numerical results. This might have stemmed from repeated buckling tests used in the present test program to generate the experimental interaction curve, which could have introduced residual strains/deformations in the skin that influenced the skin buckling load capacity, thus yielding a lower first skin buckling load in the subsequent loading stages.

Nomenclature

E_{11}	=	Young's modulus in the principal direction
E_{22}	=	Young's modulus in the minor direction
G_{12}	=	shear modulus
L	=	total length
L_{al}	=	arc length
L_n	=	nominal length
P_{const}	=	constant axial compression
P_{cr}	=	critical axial compression
R	=	panel radius
T_{const}	=	constant torque
T_{cr}	=	critical torque
υ_{12}	=	major Poisson's ratio

I. Introduction

LOADING of single curved panels (which represent a nonsymmetric structure) in buckling tests poses a tough problem, particularly when they represent a segment of a structure; for example, fuselage and conclusions from the tests have to be drawn for the full structure. Therefore, although being much more expensive in testing, it is more appropriate to test symmetric closed-type structures that consist of two or more identical panels, thus avoiding nonsymmetric loading introduction difficulties. This approach was adopted in the present test program.

Experimental and theoretical investigations on the buckling and postbuckling behaviors of composite stiffened curved panels and shells are quite scarce (all of which are concerned with aerospace applications) and are barely documented in the open literature. Among these are the analytical and experimental studies carried out at the Aircraft Division of the Northrop Corporation by Agarwal [1]; at the NASA Langley Research Center by Knight and Starnes [2]; the joint programs of NASA Langley Research Center, Lockheed Engineering and Sciences Company, Boeing Commercial Airplane group, Douglas Aircraft Company, and the Alenia Company, which were reported by McGowan et al. [3] and by Bucci and Mercuria [4]; the studies conducted by Israel Aircraft Industries and the Aerospace Structures Laboratory, which are discussed in [5] (Chapter 14), and the other studies cited and discussed in detail in that reference; and the recent studies performed within the framework of the Improved Postbuckling Simulation for Design of Fibre Composite Stiffened Fuselage Structures (POSICOSS) consortium [6–15].

The present study presents the results of tests on four torsion boxes under various combinations of axial and shears loads, the local buckling of their skins, their behavior in postbuckling under combined loading, and their collapse under torsion. These tests were conducted within the framework of the POSICOSS consortium. The tests aimed at demonstrating the safe operation of postbuckled composite cylindrical stiffened panels, as well as providing part of a database for the development of fast tools for reliable design of this type of structures, which was the main goal of POSICOSS.

II. Specimens and Test Setup

Within the framework of the POSICOSS effort, Israel Aircraft Industries designed and manufactured 12 Hexcel IM7 (12K)/8552 (33%) graphite-epoxy stringer-stiffened composite panels using a cocuring process. The nominal radius of each panel was $R = 938$ mm with a total length of $L = 720$ mm (which included two end supports having the height of 30 mm, each). The nominal test length was $L_n = 680$ mm and the panel arc length was $L_{al} = 680$ mm. The

Presented as Paper 1933 at the 46th AIAA/ASME/ASCE/AHS/ASC Structures, Structural Dynamics, and Materials Conference, Austin, TX, 18–21 April 2005; received 4 September 2006; revision received 28 August 2007; accepted for publication 15 October 2007.

*Associate Professor, Faculty of Aerospace Engineering. Senior Member AIAA.
†Professor, Faculty of Aerospace Engineering. Fellow AIAA.
‡Associate Professor, Department of Aerospace Engineering. Member AIAA.

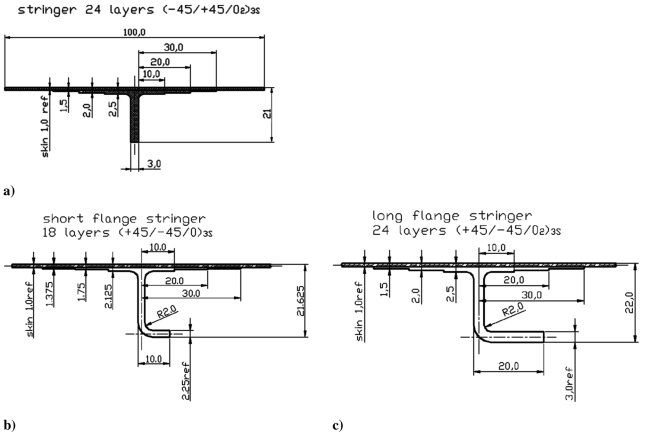

Fig. 1 Dimensions, geometry, and layups of the panels: a) box 1 and box 2, b) short-flange stringer, box 3, and c) long-flange stringer, box 4.

skin layup was quasi-isotropic $(0\ \text{deg}, \pm 45\ \text{deg}, 90\ \text{deg})_S$. Each layer had a nominal thickness of 0.125 mm. Eight of these panels were used to form four torsion boxes with cocured stringers. Each box consisted of two curved stringer-stiffened curved panels that were connected together by two flat nonstiffened aluminum side plates.

Boxes 1 and 2 were composed of panels with blade-type stringers (see Fig. 1a), box 3 had short-flange J-type stringers (see Fig. 1b), and box 4 had long-flange J-type stringers (see Fig. 1c). The dimensions and properties of the panels are given in Table 1.

Each panel was stiffened by five stringers, except for the panel with the long-flange J-type stringers, which had only four stringers. Because each pair of panels was tested as a part of a closed box, it was assumed that by applying a torque to the box, the two panels were subjected to identical shear. Various tests were performed with each box before reaching its collapse under torsion, including axial compression, torsion, and combinations of both loadings. For each box, the first buckling load was observed in the skin for axial compression only, torsion only, and combinations of axial compression and torsion to determine the buckling load under the particular type of loading, then a collapse test was performed under torsion only.

The four torsion boxes were tested at the structures laboratory of Politecnico di Milano, employing their controlled position and loading equipment [6] (see Fig. 2).

The way the shear stresses were introduced into the torsion boxes is schematically depicted in Fig. 3. Four aluminum blocks were bolted to the upper and lower heavy loading plates of the loading machine. The blocks were closely tightened against the aluminum loading end pieces of the boxes. Thus, when rotating the lower loading plate of the machine, the loading blocks bolted to it reacted against the lower box's end pieces and thus introduced torsion into the lower end of the box. At the same time, the aluminum loading blocks, which were bolted to the fixed upper machine loading plate, reacted against the upper box end pieces and prevented the upper end of the box from rotating. Thus, the box was exposed to a couple that introduced a torque into it and, consequently, introduced uniform shear stresses into the curved panels.

Before performing the buckling tests, a comprehensive finite element (FE) failure analysis of the torsion boxes was conducted, indicating high local stresses at the corners of each panel. Those corners were subsequently reinforced locally (outside and inside) by bonded aluminum patches (see Fig. 4). To assess the influence of the initial geometric imperfections on the buckling loads of the box, each panel was scanned using a linear variable differential transformer (LVDT) that was attached to a straight bar and could move in the longitudinal direction (see Fig. 4a). The bar rested on end pieces that provided its circumferential movement following the circumference of the panel. A three-dimensional map of imperfections was obtained, as depicted in Fig. 4b. Eliminating the imminent rigid-body degrees of freedom stemming from the measurement setup yielded the map of actual initial geometric imperfections (see Fig. 4c).

During the tests, the values of axial displacement, rotation, axial compression load, and torque of the box were measured by LVDTs and a load cell. In parallel, the strains at a priori designated points were monitored by 80 strain gauges that were bonded back to back, both on the skin and on the stringers of each panel. The strain-gauge map and the LVDT locations are shown in Fig. 5, and Fig. 6 depicts a photo of the panel with the bonded strain gauges.

III. Results

A. Experimental Results

Each torsion box underwent a series of tests aimed at construction of the first skin buckling interaction curve of combined axial compression and torsion-carrying capability. At the beginning of each test and before reaching the first skin buckling, the circumferential load distribution, either under axial compression or under torsion, as reflected by the strain gauges (mainly by those along the middle line between the end pieces) was recorded and loading was adjusted accordingly, to achieve the best uniform loading, thus diminishing (as much as possible) eccentricity and/or nonuniform loading, which might have affected the buckling capacity of the box and lead to misleading results.

Tables 1–5 and Figs. 7a–7d summarize the experimentally observed buckling loads of the four torsion boxes included in the present test program. Note that the reported values in the tables,

Table 1 Data used for load calculations of torsion boxes 1–4

	Stringer type		
	Blade	Short-flange J	Long-flange J
Specimens	Box 1, box 2	Box 3	Box 4
Total panel length	720 mm	720 mm	720 mm
Free panel length	660 mm	660 mm	660 mm
Radius	938 mm	938 mm	938 mm
Arc length	680 mm	680 mm	680 mm
Number of stringers	5	5	4
Stringer distance	136 mm	136 mm	174 mm
Laminate layup of skin	$[0\ \text{deg}, 45\ \text{deg}, -45\ \text{deg}, 90\ \text{deg}]_S$	$[0\ \text{deg}, 45\ \text{deg}, -45\ \text{deg}, 90\ \text{deg}]_S$	$[0\ \text{deg}, 45\ \text{deg}, -45\ \text{deg}, 90\ \text{deg}]_S$
Laminate layup of stringer	$[45\ \text{deg}, -45\ \text{deg}, 0_2\ \text{deg}]_{3S}$	$[45\ \text{deg}, -45\ \text{deg}, 0\ \text{deg}]_{3S}$	$[45\ \text{deg}, -45\ \text{deg}, 0_2\ \text{deg}]_{3S}$
Ply thickness	0.125 mm	0.125 mm	0.125 mm
Type of stringer	Blade	J-stringer	J-stringer
Stringer height	20 mm	20.5 mm	20.5 mm
Stringer feet width	60 mm	60 mm	60 mm
Stringer flange width	—	10 mm	20 mm
E_{11}	$147,300\ \text{N/mm}^2$	$147,300\ \text{N/mm}^2$	$147,300\ \text{N/mm}^2$
E_{22}	$11,800\ \text{N/mm}^2$	$11,800\ \text{N/mm}^2$	$11,800\ \text{N/mm}^2$
G_{12}	$6000\ \text{N/mm}^2$	$6000\ \text{N/mm}^2$	$6000\ \text{N/mm}^2$
ν_{12}	0.3	0.3	0.3

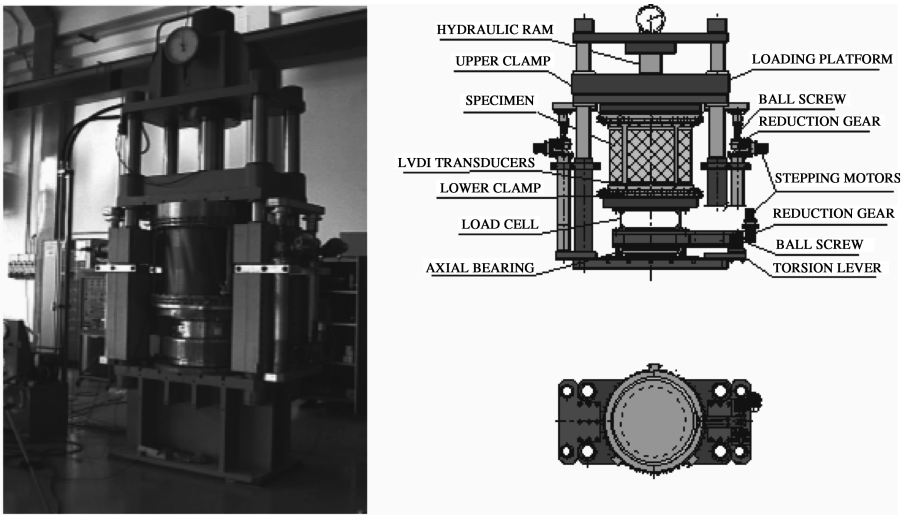

Fig. 2 Loading equipment at the laboratory of Politecnico di Milano.

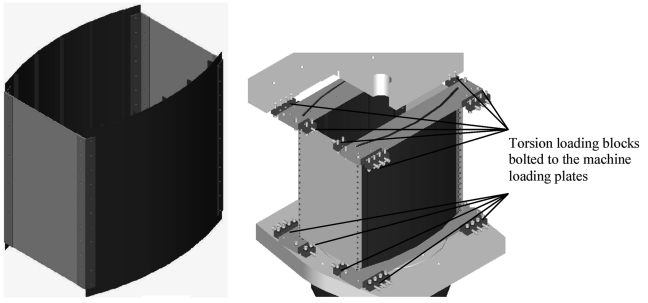

a) **b)**

Fig. 3 Schematic drawing of the torsion box: a) the box with two curved panels and two straight side aluminum plates b) the mechanism of transferring the torque into the curved stringer-stiffened panels.

either axial compression or torsion, correspond to the whole torsion box. To find the result for a single panel, the value should be divided by two.

One should note that the experimental buckling load was defined as the load at which the first buckle appeared, and in almost all cases, these buckling loads were associated with the appearance of a local single buckle. This is in contrast to the FE calculations, which are based on the eigenvalue method to yield the first buckling load, thus presenting a well-developed map of buckles.

Box 1 was the first to be tested within the present reported test program. Panel A buckled first under axial compression at 120.3 kN, followed by buckling of panel B at 134 kN. These results are in good agreement with the results reported in [6] (see also Table 2) for panels PSC 1, PSC 2, and PSC 4: namely, 131, 150, and 158.5 kN, respectively. After releasing the axial compression, the box was tested on the counterclockwise (CCW) pure torsion, followed by a pure clockwise (CW) torsion. Then it was subjected to seven different combinations of constant torsion and buckling under axial compression and, vice versa, constant axial compression and buckling under torsion. Finally, the box was subjected to a small initial axial compression load (12 kN) and collapsed under torsion. The collapse torque was experienced at 47.4 kNm with $P_{const} = 18.5$ kN for both panels (see Table 2). Note that due to the box warping, the constant axial compression could not be maintained and its value increased. In the postbuckling region, as expected, oblique short waves were encountered on the skin of both panels, which transformed into long waves, ranging from the upper to the bottom end plates, when approaching collapse. The postbuckling region was found to be very significant: 3.792 times the first buckling load. The collapse was characterized by a sudden loud noise accompanied by the sound of the breakage of fibers and was visually found at the corners of the box. Deep postbuckling oblique buckling waves were encountered.

The second box tested was box 2, a twin of box 1. Like box 1, it was first buckled under axial compression at 115.5 kN for panel A (see Table 3). This buckling value fairly compares with the results of box 1 (120.3 and 134 kN), as well the results of [6], previously shown and discussed for the twin box. After that, it was buckled by a pure CCW torque and subsequently by a pure CW torque. Then the box was subjected to five combinations of loads and buckled to yield a critical torque under constant axial compression and a critical axial buckling load under constant torsion. Finally, the box was subjected to an axial compression of 180 kN and collapsed in the torsion of both panels, under a torque of 48 kNm and $P_{const} = 182$ kN (see Table 3). In this case, the initial constant axial compression could be maintained, because under its high value, the box warping was almost not felt. Loud noise accompanied the collapse, with the sound of the breakage of fibers, which was visually found in the vicinity of the box corners.

The third box, box 3 with panels stiffened by small J-type stringers, was next tested. Unlike the previous two boxes, box 3 was first buckled under CCW pure torsion, yielding $T_{cr} = 12.8$ kNm for panel A, followed by a pure CW torsion, where $T_{cr} = 15$ kNm for panel A, followed by $T_{cr} = 20$ kNm for panel B. The third test was under axial compression, yielding 75 kN for panel A, followed by the buckling of panel B at 100 kN. These results are comparable with the results reported in [11] (see also Table 4), corresponding to panels axial 1 and axial 2: namely, 85 and 75 kN, respectively. Three more combinations of axial compression and torsion followed. The box was next tested till collapse under CCW torque (with a constant initial axial compression of 16 kN), yielding $T_{collapse} = 51.2$ kNm and $P_{const} = 21.3$ kN for both panels. Note that, as before, the constant axial compression could not be maintained and, due to the box warping, its value increased. The collapse was accompanied by a large noise from the breakage of fibers without visible damage.

Box 4 was the last box tested within the present test program. It consisted of two panels stiffened by four large J-type stringers. The first test was under axial compression, yielding a buckling of 57.5 kN for both panels (see Table 5), which is quite comparable with the results reported in [11] (see also Table 5) for panels axial 3 and axial 4: namely, 60 and 92.6 kN, respectively. Next, box 4 was buckled under CCW pure torsion, yielding $T_{cr} = 8$ kNm for both panels, followed by a pure CW torsion with critical values of $T_{cr} = 16$ kNm for panel B, followed by $T_{cr} = 22$ kNm for panel A. Next, the box was subjected to seven combinations of torsion and axial compression, yielding first buckling under either axial compression with constant torsion or vice versa. In the last test, the box was loaded under constant initial axial compression of 10 kN and collapsed under a torsion at $T_{collapse} = 69$ kNm and $P_{const} = 15$ kN for both panels. Like before, the initial constant axial compression

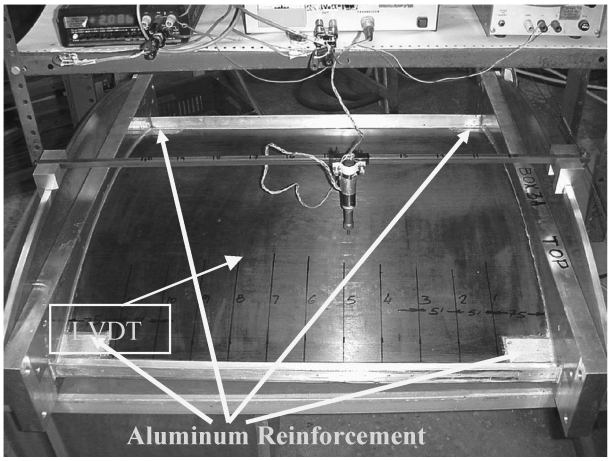

a)

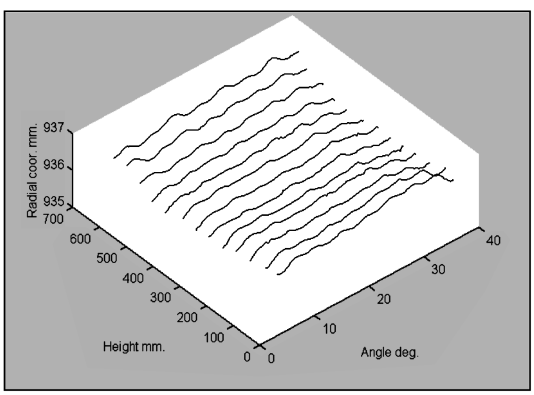

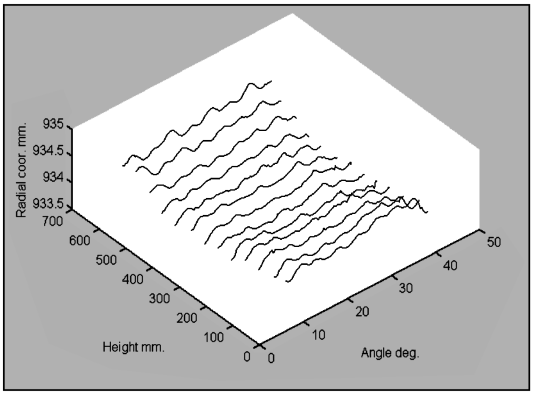

b) c)

Fig. 4 Panel A of box 3: a) setup for measurement of initial geometric imperfections-note the four aluminum reinforcements at the corners of the panel b) measured initial geometric imperfection map, and c) adjusted geometric imperfection map.

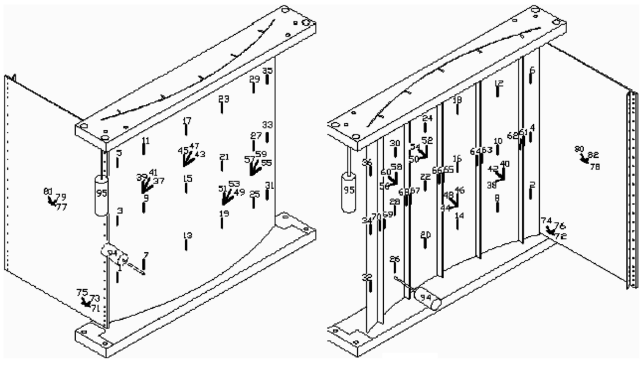

a) b)

Fig. 5 Typical strain gauges and LVDT locations: a) external view and b) internal view.

Fig. 6 Panel with a side aluminum plate and bonded strain gauges.

could not be maintained and, due to the box warping, its value increased. As experienced in the previous tests, the collapse was accompanied by a large noise and sounds of the breakage of fibers, without visible damage.

A comparison among the first buckling experimental loads with other available experimental results and numerical calculations is shown in Table 6. For buckling under axial compression, the panels A and B of boxes 1 and 2 are 14% lower than with the average buckling loads of the panels reported in [6] and are in good agreement with the various FE calculations. The panels of box 3 are 9.4% higher than the experimental results of single panels that buckled under axial compression and reported in [11] and are 12.5% lower than the FE calculations, whereas the panels of box 4 are 25% lower than those reported in [11] and 47.7% lower than the FE predictions.

When comparing the first buckle under torque, the comparison shows the same trend. Boxes 1 and 2 are 14% lower than Abaqus/Explicit results for CCW torque and 8.8% higher when applying a CW torque. Box 3 is 27% lower than with MSN.Nastran for CWW torque and 9.3% higher for CW torque, whereas for box 4, the experimental result for CCW torque is very low compared with the MSN.Nastran prediction (by 75%), and for CW, the result is very good: 1% lower than the FE predictions.

Table 2 Experimental buckling loads and collapse torque: box 1

Test No.	Initial P const, kN[a]	Initial T const, kNm[a]	Panel A Pcr, kN,[a] or $T_{collapse}$, kNm	Panel B Pcr, kN,[a] or Tcr, kNm[a] or $T_{collapse}$, kNm	Remarks	Comparable with results on single panels [6]
1	0	0	$P_{cr} = 240.6$	$P_{cr} = 268$	Axial compression test	PSC 1: 131 kN; PSC 2: 150 kN; PSC 4: 158.5 kN
2	11	0	——	$\mathbf{T_{cr} = 12.5}$ ($P_{const} = 10.5$)	CCW pure torsion test	——
3	11	0	——	$\mathbf{T_{cr} = 13.0}$ ($P_{const} = 13.3$)	CW pure torsion test	——
4	0	9 (CCW)	$\mathbf{P_{cr} = 54.5}$ ($T_{const} = 9$)	$\mathbf{P_{cr} = 34}$ ($T_{const} = 9$)	Constant torsion, buckling under axial compression	——
5	0	6 (CCW)	——	$\mathbf{P_{cr} = 85}$ ($T_{const} = 6$)	Constant torsion, buckling under axial compression	——
6	0	3 (CCW)	——	$\mathbf{P_{cr} = 190}$ ($T_{const} = 3$)	Constant torsion, buckling under axial compression	——
7	85	0	——	$\mathbf{T_{cr} = 5.2}$ ($P_{const} = 85$)	Constant axial compression, buckling under CCW torsion	——
8	34	0	——	$\mathbf{T_{cr} = 7.6}$ ($P_{const} = 34$)	Constant axial compression, buckling under CCW torsion	——
9	12	0	$\mathbf{T_{collapse} = 47.4}$ ($P_{const} = 18.5$)	$\mathbf{T_{collapse} = 47.4}$ ($P_{const} = 18.5$)	Collapse under CCW torsion with a small axial compression	——

[a]Axial compression or torsion for the whole torsion box. To find the result for a single panel, the value should be divided by 2.

Table 3 Experimental buckling loads and collapse torque: box 2

Test No.	Initial P const, kN[a]	Initial T const, kNm[a]	Panel A Pcr, kN,[a]or $T_{collapse}$, kNm	Panel B Pcr, kN,[a] or Tcr, kNm[a]or $T_{collapse}$, kNm	Remarks	Comparable with results on single panels [6]
1	0	0	$P_{cr} = 231.0$	——	Axial compression test	PSC 1: 131 kN; PSC 2: 150 kN; PSC 4: 158.5 kN
2	15	0	——	$\mathbf{T_{cr}} = 14.0$ ($P_{const} = 16.2$)	CCW pure torsion test	——
3	15	0	——	$\mathbf{T_{cr} = 18.0}$ ($P_{const} = 18.0$)	CW pure torsion test	——
4	60	0	$\mathbf{T_{cr} = 12.0}$ ($P_{const} = 60$)	$\mathbf{T_{cr} = 12.0}$ ($P_{const} = 60$)	Constant axial compression, buckling under CCW torsion	——
5	120	0	$\mathbf{T_{cr} = 7.4}$ ($P_{const} = 120$)	$\mathbf{T_{cr} = 7.4}$ ($P_{const} = 120$)	Constant axial compression, buckling under CCW torsion	——
6	180	0	$\mathbf{T_{cr} = 4.0}$ ($P_{const} = 180$)	——	Constant axial compression, buckling under CCW torsion	——
7	180	0	$\mathbf{T_{collapse} = 48.0}$ ($P_{const} = 182$)	$T_{collapse} = 48.0$ ($P_{const} = 182$)	Collapse under CCW torsion with a large axial compression	——

[a]Axial compression or torsion for the whole torsion box. To find the result for a single panel, the value should be divided by 2.

Table 4 Experimental buckling loads and collapse torque: box 3

Test No.	Initial P const, kN[a]	Initial T const, kNm[a]	Panel A Pcr, kN,[a]or $T_{collapse}$, kNm	Panel B Pcr, kN,[a]or Tcr, kNm[a]or $T_{collapse}$, kNm	Remarks	Comparable with results on single panels [11]
1	15	0	$\mathbf{T_{cr} = 12.8}$ ($P_{const} = 13.5$)	——	CCW pure torsion test	——
2	15	0	$\mathbf{T_{cr} = 15.0}$ ($P_{const} = 16.2$)	$\mathbf{T_{cr} = 20.0}$ ($P_{const} = 16.3$)	CW pure torsion test	——
3	0	0	$\mathbf{P_{cr} = 150.0}$	$\mathbf{P_{cr} = 200}$	Axial compression test	axial 1: 85 kN; axial 2: 75 kN
4	0	4 (CCW)	$\mathbf{P_{cr} = 87.0}$ ($T_{const} = 4$)	——	Constant torsion, buckling under axial compression	——
5	0	7.5 (CCW)	$\mathbf{P_{cr} = 65.0}$ ($T_{const} = 7.5$)	$\mathbf{P_{cr} = 68.0}$ ($T_{const} = 7.5$)	Constant torsion, buckling under axial compression	——
6	0	11 (CCW)	$\mathbf{P_{cr} = 50.6}$ ($T_{const} = 7.5$)	$\mathbf{P_{cr} = 50.6}$ ($T_{const} = 7.5$)	Constant torsion, buckling under axial compression	——
7	16	0	$\mathbf{T_{collapse} = 51.2}$ $P_{const} = 21.3$	$T_{collapse} = 51.2$ $P_{const} = 21.3$	Collapse under CCW torsion with a small axial compression	——

[a]Axial compression or torsion for the whole torsion box. To find the result for a single panel, the value should be divided by 2.

Table 5 Experimental buckling loads and collapse torque: box 4

Test No.	Initial P const, kN[a]	Initial T const, kNm[a]	Panel A Pcr, kN,[a]or $T_{collapse}$, kNm	Panel B Pcr, kN,[a]or Tcr, kNm[a]or $T_{collapse}$, kNm	Remarks	Comparable with results on single panels [11]
1	0	0	$P_{cr} = 115.0$	$P_{cr} = 115.0$	Axial compression test	Axial 3: 60 kN; axial 4: 92.6 kN
2	10	0	$\mathbf{T_{cr} = 8.0}$ ($P_{const} = 10.0$)	$\mathbf{T_{cr} = 8.0}$ ($P_{const} = 10.0$)	CCW pure torsion test	——
3	10	0	$\mathbf{T_{cr} = 22.0}$ ($P_{const} = 10.0$)	$\mathbf{T_{cr} = 16.0}$ ($P_{const} = 10.0$)	CW pure torsion test	——
4	0	4 (CCW)	$\mathbf{P_{cr} = 70.0}$ ($T_{const} = 4$)	$\mathbf{P_{cr} = 50.0}$ ($T_{const} = 4$)	Constant torsion, buckling under axial compression	——
5	0	2 (CCW)	$\mathbf{P_{cr} = 80.0}$ ($T_{const} = 2$)	$\mathbf{P_{cr} = 74.0}$ ($T_{const} = 2$)	Constant torsion, buckling under axial compression	——
6	0	6 (CCW)	$\mathbf{P_{cr} = 50.0}$ ($T_{const} = 6$)	$\mathbf{P_{cr} = 60.0}$ ($T_{const} = 6$)	Constant torsion, buckling under axial compression	——
7	60	0	$\mathbf{T_{cr} = 5.4}$ ($P_{const} = 60$)	$\mathbf{T_{cr} = 3.0}$ ($P_{const} = 60$)	Constant axial compression, buckling under CCW torsion	——
8	0	8 (CW)	$\mathbf{P_{cr} = 130.0}$ ($T_{const} = 8$)	$\mathbf{P_{cr} = 121.0}$ ($T_{const} = 8$)	Constant torsion, buckling under axial compression	——
9	0	12 (CW)	$\mathbf{P_{cr} = 126.0}$ ($T_{const} = 12$)	$\mathbf{P_{cr} = 70.0}$ ($T_{const} = 12$)	Constant torsion, buckling under axial compression	——
10	0	4 (CW)	$\mathbf{P_{cr} = 120.0}$ ($T_{const} = 4$)	$\mathbf{P_{cr} = 130.0}$ ($T_{const} = 4$)	Constant torsion, buckling under axial compression	——
11	10	0	$\mathbf{T_{collapse} = 69.0}$ $P_{const} = 15$	$\mathbf{T_{collapse} = 69.0}$ $P_{const} = 15$	Collapse under CCW torsion with a small axial compression	——

[a]Axial compression or torsion for the whole torsion box. To find the result for a single panel, the value should be divided by 2.

Table 6 First buckling loads as predicted by the various FE codes for boxes 1–4 and experimental values

FE code	Box 1 and box 2			Box 3			Box 4		
	P_{cr}, kN[d]	T_{cr}^{CCW}, kNm	T_{cr}^{CW}, kNm	P_{cr}, kN[d]	T_{cr}^{CCW}, kNm	T_{cr}^{CW}, kNm	P_{cr}, kN[d]	T_{cr}^{CCW}, kNm	T_{cr}^{CW}, kNm
MSC.Nastran[a]	120.52	17.57	−16.27	100.92	17.52	−16.01	110.60	22.08	−19.21
Abaqus/Implicit[a]	120.33	16.18	−15.30	98.45	16.15	−15.10	109.70	21.33	−18.12
Abaqus/Explicit[b]	120.05	15.41	−14.24	——[c]	15.28	——[c]	——[c]	20.87	——[c]
Average: panels PSC 1, PSC 2, and PSC 4 [6]	146.5	——	——	——	——	——	——	——	——
Average: panels A and B and boxes 1 and 2	123.27	13.25	15.5	——	——	——	——	——	——
Average: panels axial 1 and axial 2 [11]	——	——	——	80	——	——	——	——	——
Average: panels A and B and box 3	——	——	——	87.5	12.8	17.5	——	——	——
Average: panels axial 3 and axial 4 [11]	——	——	——	——	——	——	76.3	——	——
Average: panels A and B and box 4	——	——	——	——	——	——	57.5	8	19

[a]Linear.
[b]Nonlinear.
[c]Three-CPU time limit.
[d]For a single panel.

Comparison of the results observed for the four torsion boxes demonstrates the expected result that the collapse torsion-carrying capability is dependent on stringer geometry and layup. The higher the torsion rigidity of the stringers, the higher the collapse loads under torsion (see box 4 in comparison with box 3). Concerning the first buckling load under pure axial compression, or pure torsion, spacing of the stringers and their rigidity both in bending and torsion influence the first buckling of the panel. The higher the rigidity and smaller the distance between stringers, the higher the buckling load.

Typical measurements of recorded strain gauges in the tests are given in Fig. 8. Figure 8 presents the results experienced by three pairs of strain gauges (for reference, see Fig. 5) bonded on panel A of box 1: gauges 25 and 26 on the skin closer to the lower edge of the panel, gauges 29 and 30 on the skin near the upper end of the panel, and gauges 63 and 64 located at the middle of the fifth blade-type stringer. The results (see Table 2) are presented for axial compression only (test 1), clockwise torsion only (test 3), and combined axial compression and counterclockwise torsion (test 6) in Figs. 8a–8c, respectively. For comparison, the strain-gauge readings of the counterpart panel B of box 1 are also presented in Figs. 8d–8f under the same combinations of loading. Note that to conduct a correct comparison for the case of torsion only (test 3), the readings of strain gauges 7–8, 11–12, and 69–80 of panel B were compared with their counterpart strain gauges 25–26, 29–30, and 63–64 (see Fig. 5), respectively. As one can see, the readings of the strain gauges on both panels A and B of box 1 seem very similar, thus indicating that introduction of the loads into both panels was equal and balanced.

Moiré fringes, as shown in Fig. 9, were used to detect and identify the buckling and postbuckling patterns of each panel. Figures 9a–9h present the behavior and the associated changes in deformation patterns that were observed with increase in load in the tests of box 4.

Figures 10a and 10b present typical postbuckling wave patterns (see the annotations on the figures) just after collapse that were observed for panels A and B of box 2. All of the collapse loads were performed under torsion, with a small axial compression being applied on the box to prevent tearing of the connecting bolts (see Fig. 3). The collapse was characterized by a sudden loud noise accompanied by the sound of the breakage of fibers and was visible only for box 1 and box 2 at the corners of the box. Deep postbuckling oblique buckling waves were encountered.

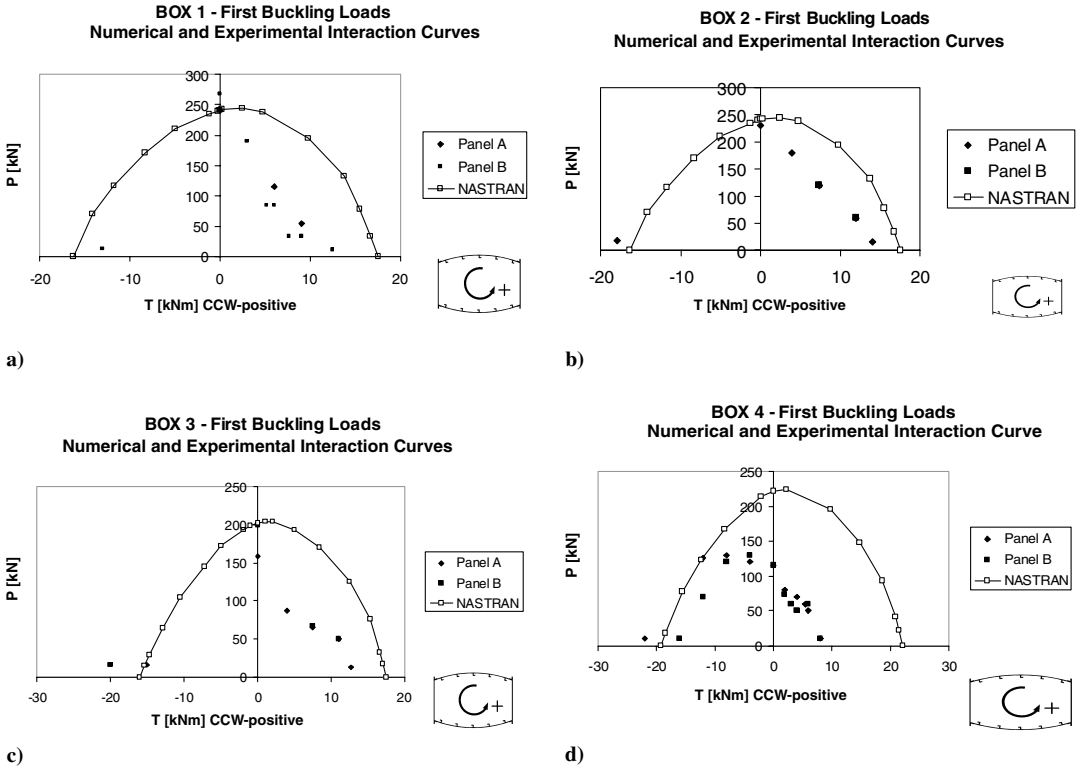

Fig. 7 Typical experimental (first skin buckling) and numerical (eigenvalue predictions) interaction curves: a) box 1, b) box 2, c) box 3, and d) box 4.

B. Numerical Results and Comparisons

The Krumbein Aerospace Structures Laboratory at the Faculty of Aerospace Engineering at the Technion—Israel Institute of Technology uses two well-known FE programs: the MSC.Nastran and the Abaqus (both Implicit and Explicit). Therefore, the numerical results presented throughout the paper are based on those codes. MSC.Nastran was mainly used, due to its modest use of computer resources, whereas Abaqus was applied for nonlinear postbuckling and collapse calculations. A common FE model was constructed and used for both codes. The refined FE model aimed at increasing the accuracy of the numerical predictions is presented in Fig. 11. Typical numerical results as yielded by this model using the Abaqus/Explicit are presented in Table 6 and compared with the linear results predicted by MSC.Nastran and Abaqus/Implicit. As expected, the MSC.Nastran predictions are consistently higher than the Abaqus predictions. This model was employed for the numerical predictions of Figs. 7a–7d. The finite element model accurately represented the connections and the stiffening of the side flat aluminum panels, as can be seen in Fig. 12. To simulate the connections and the stiffening of the side flat aluminum panels (see Fig. 12), four rows of nodes (three rows of elements) at the bottom part of the composite panels were clamped, whereas four rows of nodes at the upper part of the panel (three rows of elements) were connected together to form a rigid body with a reference node at the center of the box (see Fig. 11). The axial force and the torsion moment were applied at this reference node. The side flat aluminum panels were 3.3 mm thick and were connected with the composite panels 7 mm beneath the rigid body, so that no direct axial force was introduced into them during loading (see detail I and view A of Fig. 11). All of the elements constituting the model were four-node quadrilateral shell-type elements. Boxes 1 and 2 consisted of 11,096 elements, and boxes 3 and 4 consisted of 11,816 elements and 10,872 elements, respectively.

As already mentioned in the previous subsection, the experimentally observed and numerically predicted interaction curves for the first buckling loads of boxes 1–4 (skin buckling) were presented in Figs. 7a–7d. One should note the asymmetry of the numerical interaction curve calculated by MSC.Nastran FE that even exists for the blade-type stringer-stiffened panels of box 1 and box 2 (Figs. 7a and 7b). Because of the layup of the panel's skin, the +45-deg plies are further from the skin midplane than are the −45-deg plies (see Table 1), which leads to the different buckling loads under CCW and CW shear loading. However, this asymmetry was barely experienced during the tests on these torsion boxes. This asymmetric behavior was anticipated to a larger extent for the panels with nonsymmetric J-type stiffeners; indeed, it was more noticeable in the tests with box 3 with the smaller J-type stiffeners (Fig. 7c), and it was quite emphasized in the tests of box 4 with the large J-type stringers (Fig. 7d).

Apparently, a noticeable discrepancy is observed between the FE predictions and the test-experienced results. This disagreement requires further discussion, particularly on the testing procedures and their possible effects on the comparison with analysis.

For all of the four tested torsion boxes, good agreement of test results with numerical predictions was found for both pure unidirectional compression and torsion loadings. However, under combined loading, the experimentally observed loading combinations were lower than the calculated combinations. This observation might have resulted from the repeated buckling test procedure that was employed in the present tests to construct the experimental first buckling interaction curve, which could have introduced undetected residual strains/deformations in the panels' skins when conducting the tests for determination of each critical point of the interaction curve. Consequently, each subsequent combination of loading might have been associated with a different, more pronounced, shape of initial geometric imperfections and might even contain imperfections in the shape of one or more minor local buckles. Hence, when reloading, the box became more imperfection-sensitive, and the augmented imperfections shape could have triggered an earlier appearance of the first local buckle. One should note that similar phenomena might have occurred when changing from one type of load to another when applying combined loading. Deformations that develop under one type of loading may constitute an initial shape of geometric imperfections when maintaining this load at a constant value and when applying the other increasing component of loading till the appearance of first buckling. This procedure might also introduce enhanced imperfection-sensitivity loading to a reduction in the first skin buckling capacity. Obviously, first buckling was experimentally determined at a rather early stage of loading, compared with the MSC.Nastran eigenvalue calculations, which are incapable of catching the development of local deformations and

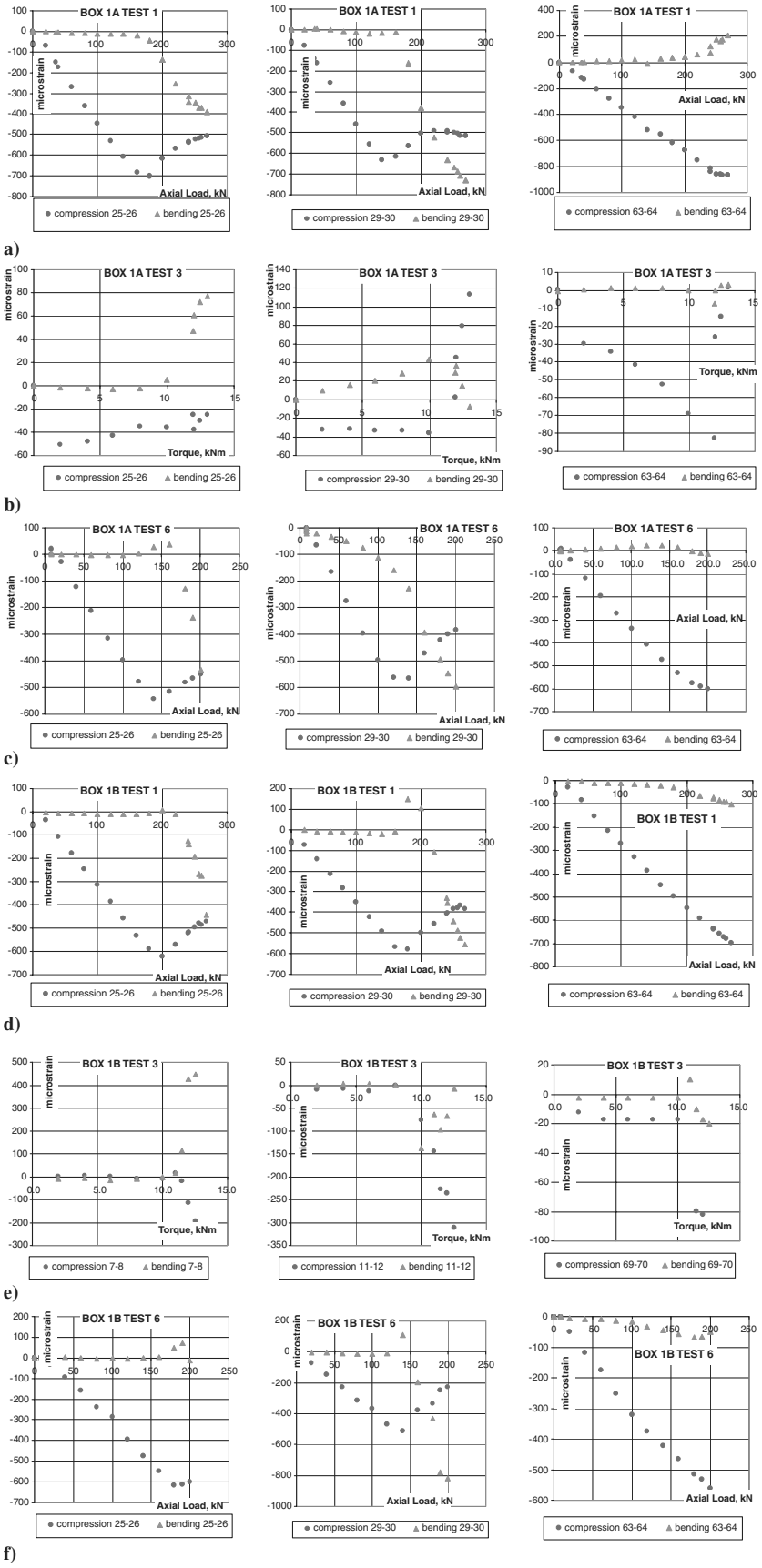

Fig. 8 Typical strain-gauge measurements for axial compression and torsion: a) test 1, b) test 3, c) test 6 panel A box 1; d) test 1, e) test 3, and f) test 6 panel B box 1.

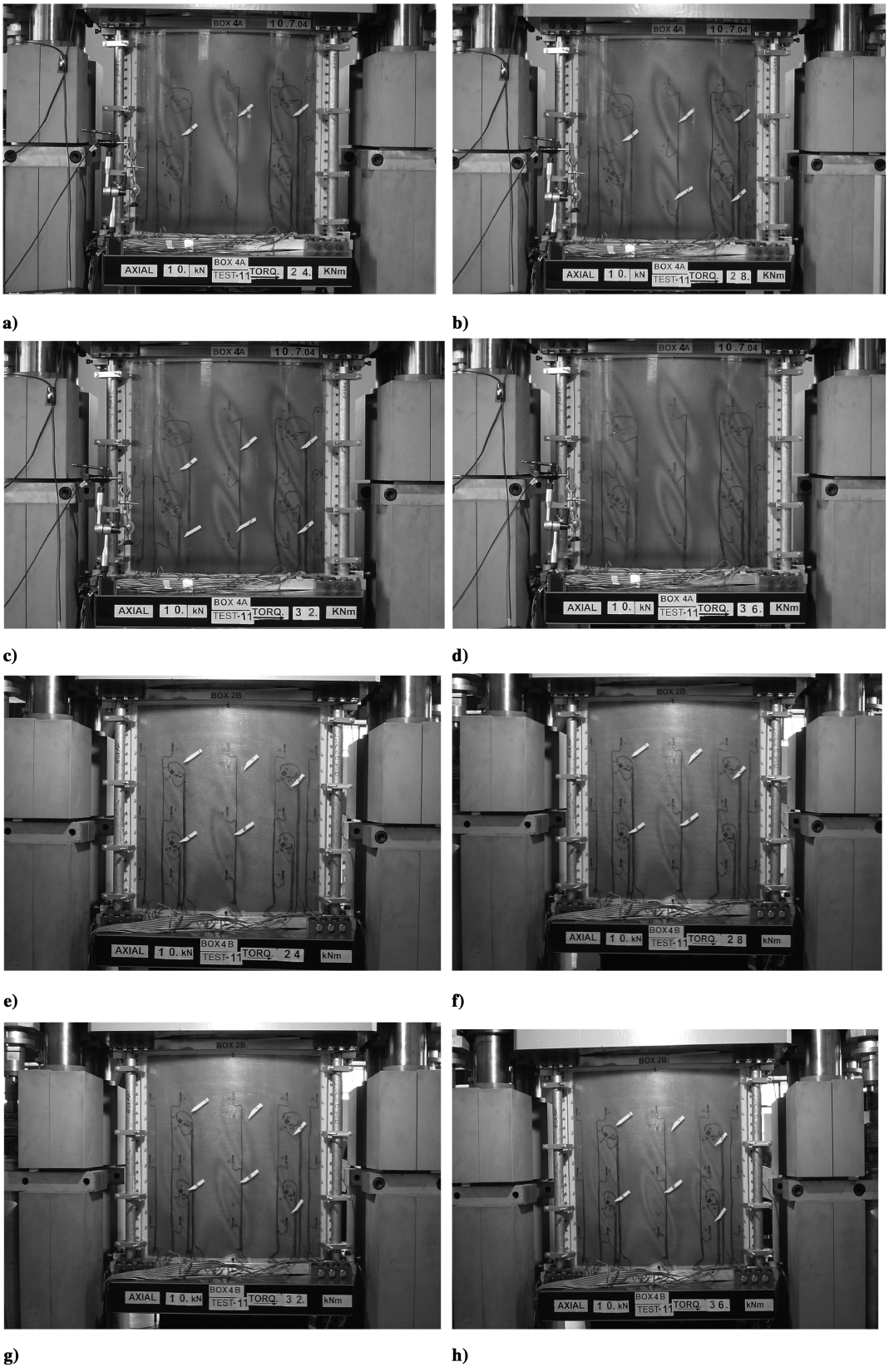

Fig. 9 Typical postbuckling patterns in test 11 of box 4, constant axial compression 10 kN and increasing torque: a–d) panel A at 24, 28, 32, and 36 kNm and f–h) panel B at 24, 28, 32 and 36 kNm.

augmentation of geometric imperfections responsible for the appearance of first skin buckling. These significant differences between experimental determination of first skin buckling and FE buckling predictions are reflected in Figs. 7a–7d.

Moreover, MSC.Nastran results were found to predict 5–10% higher buckling loads than with Abaqus/Explicit predictions (see Table 6). Another important argument in comparing the test results with FE predictions is the fact that in the tests, the fully developed buckled surface was usually observed under loading combinations in which the varying components of the combinations were about 30% higher than those associated with the first skin buckling. Therefore, one should be aware that the empirical curves in Figs. 7a–7d

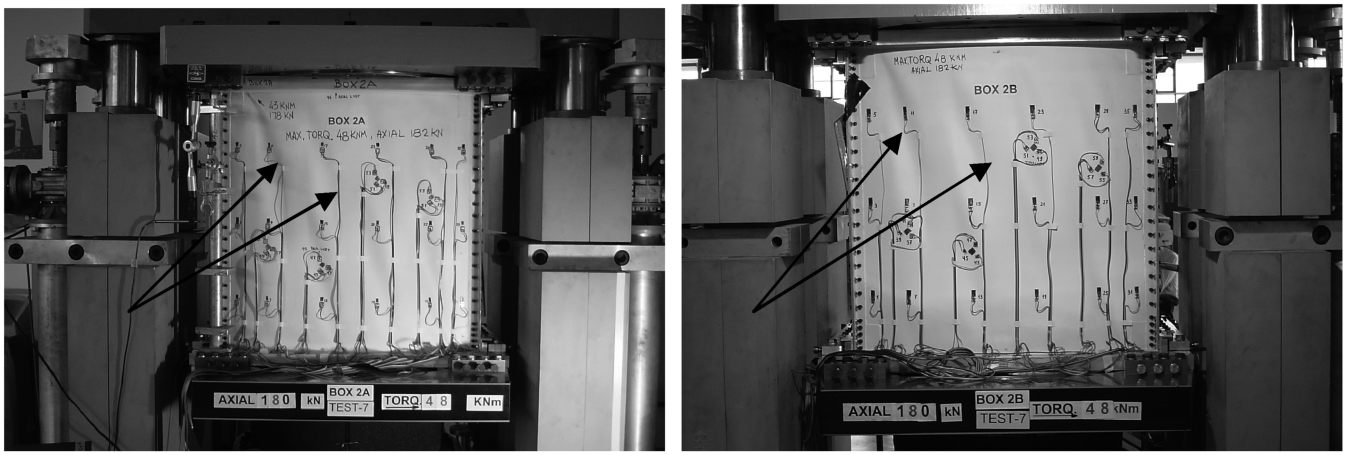

a) b)

Fig. 10 Typical wave patterns after collapse: a) panel A of box 2 and b) panel B of box 2.

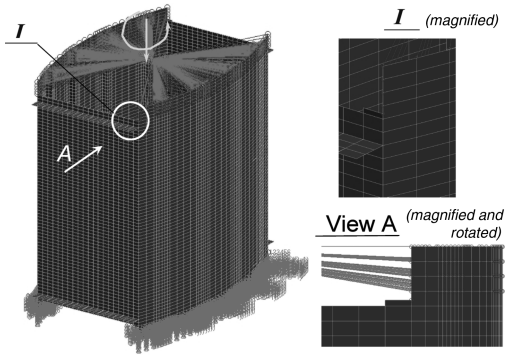

Fig. 11 Refined finite element model.

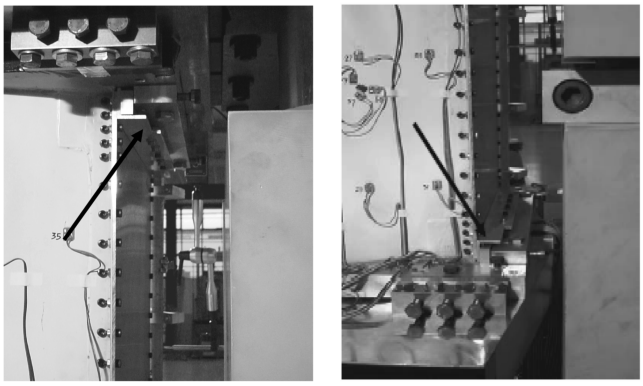

a) b)

Fig. 12 Details of the stiffening and the connections of the side flat aluminum plate: a) upper end view, b) lower end view.

represent the appearance of first skin buckling and, as such, serve only as a measure of the initiation of buckling that may occur under relative low load combinations, based on the preceding discussion, with no relevance to the box load-carrying capacity. It can be further argued that the first skin buckling is of small significance when taking into account the wide range postbuckling load-carrying capacity of the boxes before their collapse. Comparing the experimental collapse torques with those predicted by the Abaqus/Explicit FE code reveals a quite good matching: box 1, $T_{collapse,exp} = 47.4$ kNm versus $T_{collapse,FE} = 50.4$ kNm, box 3 $T_{collapse,exp} = 51.2$ kNm versus $T_{collapse,FE} = 53.8$ kNm, and box 4, $T_{collapse,exp} = 69$ kNm versus $T_{collapse,FE} = 74.2$ kNm. This only strengthens the preceding claims that the first buckling load is irrelevant and that the only important characteristic value is the collapse torque, which was shown to be well predictable. Moreover, it enhances the claim that there is no connection between the experimentally local buckling and the FE predictions based on the eigenvalue method.

The behavior of the torsion of the torsion boxes up to their collapse under torsion experienced in the tests and presented by the applied torque versus the box angle of rotation was compared with Abaqus predictions. A typical comparison is depicted in Fig. 13. Good correlation between test results and Abaqus/Explicit calculations is found from Fig. 13 (average first skin buckling under 13.25 kNm, compared with 15.41 kNm predicted by Abaqus/Explicit; collapse at 47.4 kNm, compared with 50.4 kNm predicted by Abaqus/Explicit; for further details, see Table 2). Similar results were experienced with boxes 2–4. The mode shapes associated with various critical points along the loading path of the torsion box were calculated and are shown in Fig. 13, together with the experimental points. It is worth noting that the side flat aluminum plates of the boxes did not buckle until collapse of the boxes, either in the tests or in the calculations, thus indicating their appropriate design to provide the data required and fulfilling the objectives of the present study.

It should be noted that the measured imperfections were included in the FE calculations. It was found that the amplitudes of the imperfections were in the range of less the half the thickness of the panel, and for this size of imperfections, almost no effect on the calculations was discovered.

IV. Conclusions

The deep postbuckling behavior of four torsion boxes, each comprising two stringer-stiffened cylindrical graphite-epoxy composite panels that were subjected to torsion, axial loading, and their combinations, was investigated experimentally and numerically. Detailed FE calculations assisted in identifying critical regions of the boxes. The boxes were reinforced accordingly, to avoid their premature failure. Before performing the buckling tests, the initial geometric imperfections of the two panels forming a torsion box were scanned and recorded. It was found that the amplitude of the imperfections was in the range of the thickness of the panel and, as expected, the initial geometric imperfections did not influence the buckling loads.

The tests indicated that torsion-carrying capacity is dependent on stringer geometry and layup; axial compression results were in very good agreement with previous tests performed with single identical panels; and the boxes have a very high postbuckling load-carrying capacity. Comparisons of the experimentally experienced first skin buckling and collapse torques with those predicted numerically by FE analyses were found to be in good agreement for pure torsion and axial compression. For combined loading, the experimental results were consistently lower than with the numerical results. A plausible explanation might be that the repeating buckling procedure used in

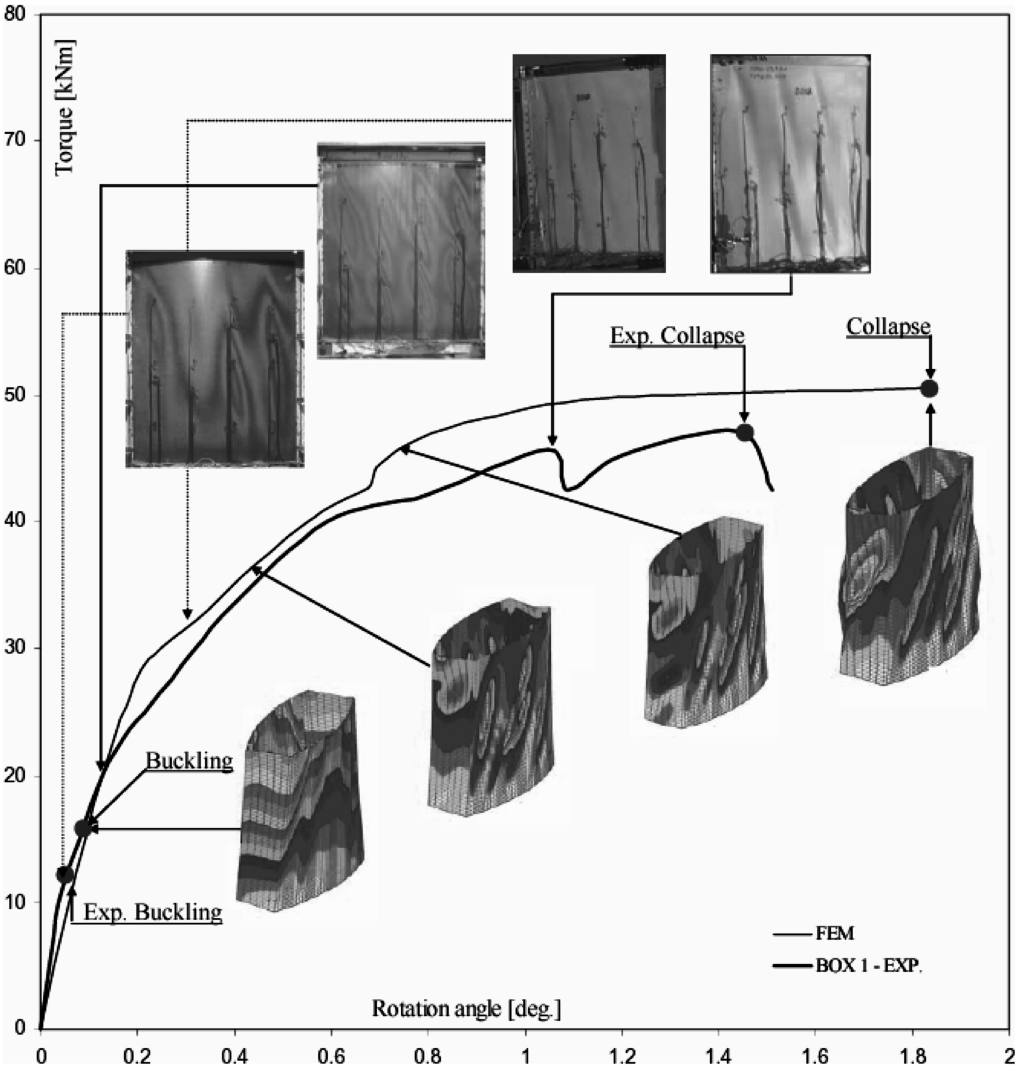

Fig. 13 Torque versus rotation-angle/Abaqus/Explicit predictions and experimental curve of box 1 (panel A).

the present test series to produce the experimental interaction curve might have induced residual strains/deformations that influenced the first skin buckling load capacity, thus yielding a lower buckling load.

The first experimentally observed skin buckling is of a very local nature and is not necessarily always an indication of the occurrence of buckling. Hence, comparison with the analysis might be inconclusive and even misleading. Because the present study deals with very deep postbuckling behavior (and with a very high reserve of load-carrying capacity beyond buckling predictions and, particularly, first skin buckling), it is suggested to compare buckling predictions with the loads corresponding to the experimentally observed first fully developed skin buckling. This will assure and enable a fair comparison that leads to more decisive and practical conclusions.

Acknowledgments

This work was partly supported by the European Commission, Competitive and Sustainable Growth Programme, contract G4RD-CT-1999-00103, with the Improved Postbuckling Simulation for Design of Fibre Composite Stiffened Fuselage Structures (POSICOSS) project. The information in this paper is provided as is and no guarantee or warranty is given that the information is fit for any particular purpose. The user thereof uses the information at their sole risk and liability. The authors would like to thank A. Grunwald, Aerospace Structures Laboratory, and P. Cordisco, Politecnico di Milano, for their exceptional assistance in setting up the tests and dedicated assistance in performing them and P. Pevsner, Aerospace Structures Laboratory, for his helpful assistance in carrying out the numerical calculations.

References

[1] Agarwal, B. L., "Post-Buckling Behavior of Composite-Stiffened Curved Panels Loaded in Compression," *Experimental Mechanics*, Vol. 22, No. 6, June 1982, pp. 231–236. doi:10.1007/BF02326363

[2] Knight, N. F. Jr., and Starnes, J. H. Jr., "Post-Buckling Behavior of Selected Curved Stiffened Graphite-Epoxy Panels Loaded in Axial Compression," *AIAA Journal*, Vol. 26, No. 3, Mar. 1988, pp. 344–352.

[3] McGowan, D. M., Young, R. D., Swancon, G. D., and Waters, W. A., "Compression Tests and Nonlinear Analysis of a Stringer- and Frame-Stiffened Graphite Epoxy Fuselage Crown Panel," *5th NASA/DoD Advanced Composite Technology Conference*, CP-3294, NASA, Washington, D.C., Aug. 1994, pp. 22–25.

[4] Bucci, A., and Mercuria, U., "CFRP Stiffened Panels Under Compression, The Utilization of Advanced Composites in Military Aircraft," AGARD Rept. 785, Neuilly sur Seine, France, 7–11 Oct. 1996, pp. 12-1–12-14.

[5] Singer, J., Arbocz, J., and Weller, T., *Buckling Experiments—Experimental Methods in Buckling of Thin-Walled Structures*, Vol. 2, Wiley, New York, 2002.

[6] Abramovich, H., Grunwald, A., Pevsner, P., Weller T., David, A., Ghilai, G., Green, A., and Pekker, N., "Experiments on Axial Compression Post-Buckling Behavior of Stiffened Cylindrical Composite Panels," 44th AIAA/ASME/ASCE/AHS Structures, Structural Dynamics, and Material Conference, Norfolk, VA; AIAA Paper 2003-1793, 2003.

[7] Bisagni, C., and Cordisco, P., "An Experimental Investigation into the Buckling and Post-Buckling of CFRP Shells Under Combined Axial and Torsion Loading," *Composite Structures*, Vol. 60, No. 4, 2003, pp. 391–402.
doi:10.1016/S0263-8223(03)00024-2

[8] Gal, E., Levy, R., Abramovich, H., and Pevsner, P., "Buckling of Composite Stiffened Panels: Analysis and Experiment," *Composite Structures*, Vol. 73, No. 2, May 2006, pp. 179–185.
doi:10.1016/j.compstruct.2005.11.052

[9] Zimmermann, R., and Rolfes, R., "POSICOSS—Improved Post-Buckling Simulation for Design of Fibre Composite Stiffened Fuselage Structures," *Composite Structures*, Vol. 73, No. 2, May 2006, pp. 171–174.
doi:10.1016/j.compstruct.2005.11.041

[10] Bisagni, C., and Cordisco, P., "Post-Buckling and Collapse Experiments of Stiffened Composite Cylindrical Shells Subjected to Axial Loading and Torque," *Composite Structures*, Vol. 73, No. 2, May 2006, pp. 138–149.
doi:10.1016/j.compstruct.2005.11.055

[11] Abramovich, H., Pevsner, P., Weller, T., Pecker, N., and Ghilai, G., "Axial Buckling of Laminated Composite Stringer-Stiffened Curved Panels—Tests vs. FE Predictions," International Conference on Buckling and Post-Buckling Behavior of Composite Laminated Shell Structures, Eilat, Israel, Faculty of Aerospace Engineering, Technion—Israel Inst. of Technology Paper 9, Mar. 2004.

[12] Zimmermann, R., Klein, H., and Kling, A., "Buckling and Post-Buckling of Stringer Stiffened Fibre Composite Curved Panels—Tests and Computations," *Composite Structures*, Vol. 73, No. 2, May 2006, pp. 150–161.
doi:10.1016/j.compstruct.2005.11.050

[13] Abramovich, H., Pevsner, P., Weller, T., and Bisagni, C., "The Behavior of Laminated Composite Stringer Stiffened Curved Panels Under Torsion Moments—Tests vs. FE Predictions," International Conference on Buckling and Post-Buckling Behavior of Composite Laminated Shell Structures, Eilat, Israel, Faculty of Aerospace Engineering, Technion—Israel Inst. of Technology Paper 10, Mar. 2004.

[14] Thomson, R. S., and Scott, M. L., "A Review of Post-Buckling Composite Aerospace Structures Research in Australia," International Conference on Buckling and Post-Buckling Behavior of Composite Laminated Shell Structures, Eilat, Israel, Faculty of Aerospace Engineering, Technion—Israel Inst. of Technology Paper 14, Mar. 2004.

[15] Falzon, B. G., and Cerini, M., "An Automated Hybrid Procedure for Capturing Mode-Jumping in Post-Buckling Composite Stiffened Structures," *Composite Structures*, Vol. 73, No. 2, May 2006, pp. 186–195.
doi:10.1016/j.compstruct.2005.11.053